I&EC research
Industrial & Engineering Chemistry Research

pubs.acs.org/IECR

Article

Novel Variable Configuration Design for Ultrahigh Recovery Reverse Osmosis Desalination of Brackish Water

Mingheng Li* and Joseph Li*

Cite This: *Ind. Eng. Chem. Res.* 2024, 63, 5813−5822

Read Online

ACCESS | Metrics & More | Article Recommendations | Supporting Information

ABSTRACT: A novel transient and cyclic design is proposed for ultrahigh recovery reverse osmosis (RO) desalination of brackish water. The designed system consists of two subsystems, a conventional multistage RO and a flow reversal and retentate recycle RO. The operation periodically switches between two different configurations, a series connection of the two subsystems for full production, and a parallel connection for partial production and flushing of the most concentrated membranes using the undersaturated fresh feed. Such a transient and cyclic design concept incorporates beneficial features of ROTEC's flow reversal RO (FRRO) and DuPont/Desalitech's closed-circuit RO (CCRO) in a single system. It offers operational flexibility at ultrahigh recoveries and requires a slight hardware modification to retrofit existing brackish water RO plants. Dynamic simulations show that concentration hotspots and overshoots are less severe than those in FRRO. It also avoids cycle-to-cycle salt buildups that are inevitable in CCRO given that it is an open-circuit design.

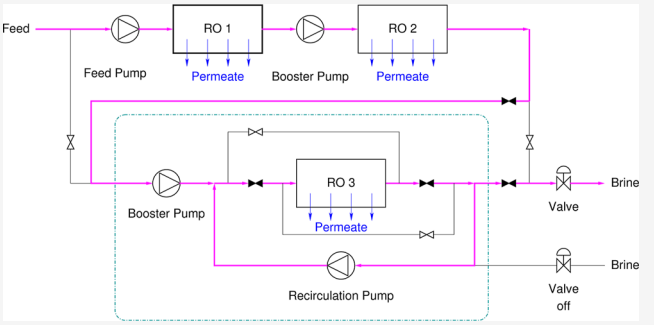

INTRODUCTION

Sustainable water supply has become a critical issue aggravated by population growth, socioeconomic development, and climate change. Desalination offers a viable solution to clean water production from saline and brackish groundwater resources.[1−3] In brackish water reverse osmosis (BWRO) plants, 2 to 3 stages are typically used, reaching a recovery of 80−85%.[4,5] The rejected brine must be disposed in accordance of local ordinances, via means including sewer discharge, deep-well injection, evaporation ponds, and marine outfall.[6] Brine management is costly, especially in inland areas.[4] Increasing the recovery rate not only enhances the water supply but also reduces the brine volume. However, the recovery rate in BWRO is usually limited by the scaling potential of sparingly soluble minerals (e.g., $CaCO_3$, $CaSO_4$, $BaSO_4$, $SrSO_4$, CaF_2, and SiO_2) in the feed.[7−11] In a traditional steady-state design, the tail-end RO elements are exposed to the highest concentration of these scalants indefinitely, unless interrupted by clean-in-place (CIP) or permeate flushing. Using antiscalants alone at high recoveries may not be very effective as they only interfere with the precipitation of salts on the membrane surface instead of stopping it, and overdosing may even cause fouling issues.[12]

One possible way to mitigate scaling at ultrahigh recoveries is a transient and cyclic operation where membranes are periodically flushed. Examples include closed-circuit RO (CCRO) or semibatch RO,[5,13−18] improved CCRO or batch RO (BRO),[15,19−24] and flow reversal RO (FRRO).[25−30] Both BRO and CCRO have a closed-circuit filtration step followed by a flushing step, while the former includes an extra volume-varying cylinder to reduce undesirable mixing in the latter. The CCRO developed by DuPont/Desalitech has been shown to be relatively resistant to fouling,[14] because the cycle time may be shorter than the crystallization induction time of most sparingly soluble salts.[16,21] A pilot study at Orange County Water District (California, United States) showed the possibility of utilizing CCRO as the fourth stage to concentrate brine from its current three-stage RO system, reaching a total recovery as high as 91%.[5]

ROTEC's FRRO is another example of transient and cyclic RO. It is based on the conventional three-stage configuration with additional periodic flow reversal and block rotation characteristics. These periodically reset the crystallization induction clock and reduce the imbalance of salt/foulant load across all stages. Therefore, it holds the promise of operating at higher recoveries than can be achieved using antiscalants alone. After completing side-by-side testing of CCRO and FRRO pilots, the Arcadia Water Treatment Plant (Santa Monica, California, United States) retrofitted its existing RO system using the FRRO technology, which is now in operation. The upgraded system has a targeted recovery of 90%, which augments approximately 10% of the current water supply

Received: December 11, 2023
Revised: March 10, 2024
Accepted: March 11, 2024
Published: March 22, 2024

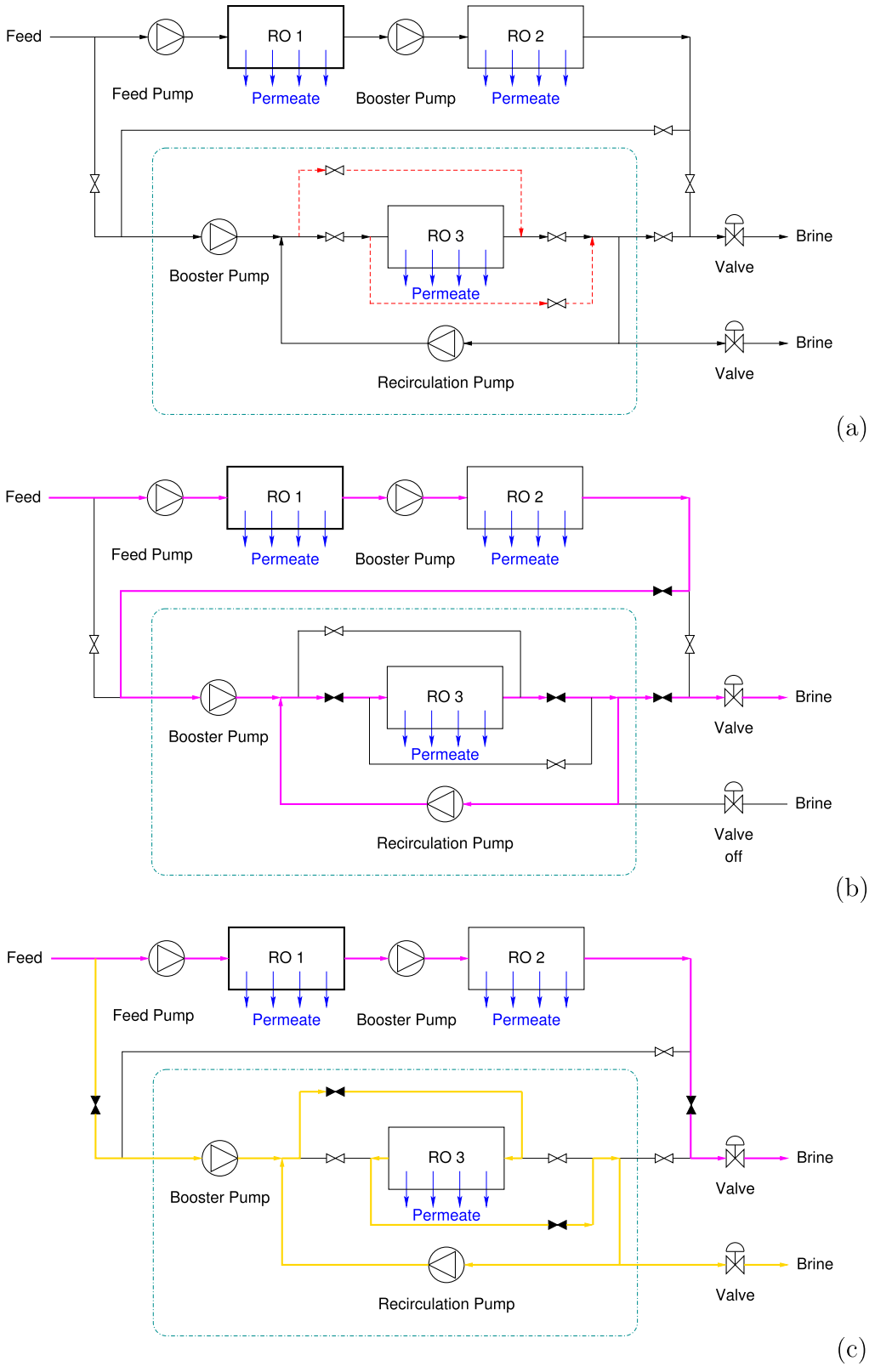

Figure 1. (a) System design with variable configurations. (b) Two subsystems arranged in series as shown by the colored thick lines. (c) Two subsystems arranged in parallel as shown by the colored thick lines.

without an increase in groundwater production. The estimated payback time for hardware modification is only two years.[31]

It is shown that the advantage of CCRO lies in maintaining the minimum feed flow per vessel and flushing membranes periodically instead of reducing specific energy consumption (SEC). Different from what was previously thought, our recent study indicates that CCRO may consume more energy than conventional multistage RO under the same design conditions for BWRO.[32] Probable causes include the following: (i) BWRO is usually operated far from the thermodynamic limit, and the

https://doi.org/10.1021/acs.iecr.3c04406
Ind. Eng. Chem. Res. 2024, 63, 5813−5822

benefit of internal staging in CCRO for energy savings is minimal; (ii) there is undesirable entropy generation due to the mixing of low-salinity feed and high-salinity recycled retentate; and (iii) there is cycle-to-cycle salt buildup because flushing is often imperfect. Moreover, given the closed-circuit nature of this technology, it is extremely sensitive to changing water quality in the pilot tests conducted at the Arcadia plant.[33] Occasionally, the pressure ceiling (set to 300 psi) was reached and the recovery rate declined continuously. FRRO is essentially a multistage RO with occasional block rotation and flow reversal occurrence and, therefore, the SEC levels in both cases are comparable. However, a significant concentration overshoot at the RO outlet was observed every time block rotation and flow reversal in stage 2 occurred at the same time.[31] How to suppress the concentration overshoot in FRRO remains an unaddressed issue.

Flow reversal and retentate recycle (FRRR) with a time-varying ratio is a new dynamic and cyclic RO design concept proposed by the authors.[34] It is a modular design that may be used as an add-on to an existing two-stage brackish water RO facility for ultrahigh RO operation. One advantage is that the viscous and mass boundary layers can be rebuilt with a larger shearing velocity when the feed flow direction is reversed. Moreover, cycle-to-cycle salt buildup inevitable in CCRO/BRO is absent in the FRRR because the latter is an open-circuit design. One drawback is that the flushing fluid is the second stage brine, which may limit its capability to "zero" the crystallization induction clock.

PROCESS DESIGN

Motivated by the above, a new transient and cyclic design, variable configuration RO (VCRO), is proposed in this work. It has two subsystems, as shown in Figure 1. One is the conventional multistage RO with interstage booster pumps. The other is the FRRR that is enclosed by the dash-dotted lines. The red dashed lines in Figure 1a indicate the option to reverse the feed direction to the FRRR stage. Depending on the operation needs, the two subsystems can be configured either in series or in parallel. In the full production mode, the two subsystems are connected in series, as shown in Figure 1b. The whole system is a typical multistage RO with optional retentate recycle in the last stage. The retentate recycle, if activated, increases the feed rate to the last stage, which helps to satisfy the minimum flow requirement per vessel for certain ultrahigh recovery applications. Under the same system recovery conditions, turning on the retentate recycle may reduce the element-level recovery and thus the risk of fouling, at the expense of a higher energy consumption.[34] The retentate recycle is somewhat analogous to the use of CCRO as an add-on module to concentrate brine from a conventional multistage RO.[5,35] In the membrane flushing mode, the two subsystems are connected in parallel, as shown in Figure 1c. The first subsystem is operated at a reduced recovery given that it has one fewer stage than the whole system. The FRRR subsystem, which has the highest salt load at the end of the full production step, is washed by the under-saturated fresh feed. The user has the option to reverse the flow and/or turn on the retentate recycle to boost the cross velocity, which thins the boundary layer and facilitates the removal of seed particles before crystallization occurs. Water flux may be on or off for the FRRR stage, similar to high or low pressure flushing in CCRO.[32] If there is no filtration flux in the flushing step, then membranes in the FRRR stage will have the least amount of salt before returning back to full production. However, the recovery in the full production step must be slightly elevated to maintain the time-average recovery. The use of fresh feed to flush the most-concentrated membranes is similar to block rotation in ROTEC's FRRO[31] as well as the adoption of a side conduit filling from the fresh feed in DuPont/Desalitech's CCRO for membrane purging.[5,35] Note that the design concept shown in Figure 1 is different from the original FRRR[34] where the membrane is flushed using brine from the preceding RO stage.

The VCRO is versatile for transient and cyclic operation. One example is shown in Table 1, which consists of four steps in one full cycle. Every time that the FRRR unit is flushed, its feed flow changes in direction. In this way, the lead and rear-end elements equally share the highest salt load during full production. Moreover, flushing of the most concentrated elements accounts for 50% of the total operation time, which facilitates the removal or dissolution of previously formed scales. An alternative operation strategy is to set the feed flow to the FRRR subsystem forward in steps 1−2 and reverse in steps 3−4.

Table 1. Cyclic Operation of VCRO

step	subsystem 1 (multistage RO)	subsystem 2 (FRRR)	connection type
1	forward	forward	in series
2	forward	reverse	in parallel
3	forward	reverse	in series
4	forward	forward	in parallel

Another advantage of VCRO is that both flow reversal and retentate recycle have been individually used in industrial RO system designs, making its development and commercialization less risky. Moreover, if the performance of the FRRR unit degrades to an unacceptable level during operation, it can be turned off and cleansed, while the remaining system can still run at a reduced recovery (e.g., 80%).

RESULTS AND DISCUSSION

A case study is presented in this section to compare VCRO and FRRO. The design conditions are listed in Table 2. The feed is based on the Chino I Desalter (California, United States) which operates at a typical recovery of 80% using a 28:14 RO array.[4] Process models have been developed and validated against high-recovery trial experiments in the range of 78−90%.[4,36,37] In this work, a third stage is added, and the system recovery is increased to 90%. It is verified that the flow rate from the last RO element is 5 m^3/h (higher than the minimum 3 m^3/h suggested by DuPont[38]) without the recycling loop at the last stage. For higher recoveries (e.g., 95%), retentate recycle may be activated

Table 2. Design Conditions

parameter	value
total feed rate (m^3/h)	346.4
overall recovery	90%
feed osmotic pressure (bar)	0.62
RO array	28:14:7
number of elements per vessel	7
RO element	BW30-400
element area (m^2)	37
membrane permeability (lmh/bar)	2.79
average flux (lmh)	24.5 (27/24/17)
feed per vessel in each stage (m^3/h)	12.4/10.8/9.3

https://doi.org/10.1021/acs.iecr.3c04406
Ind. Eng. Chem. Res. 2024, 63, 5813−5822

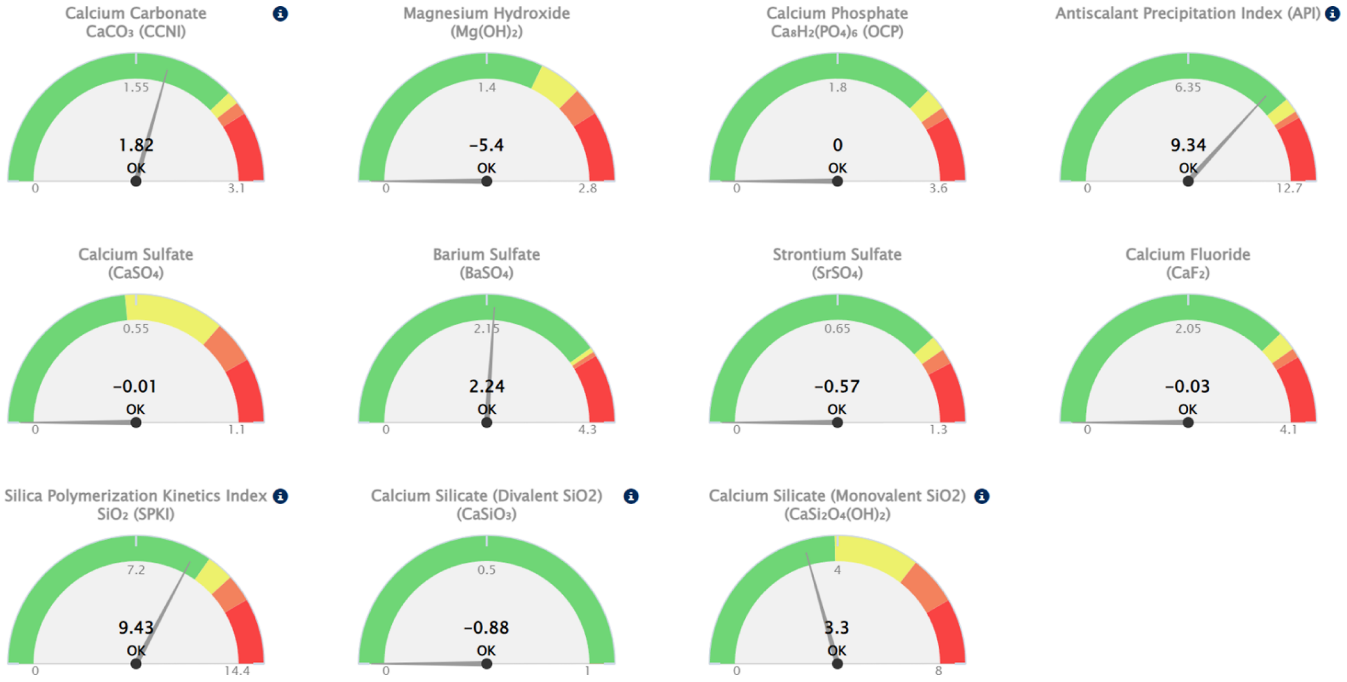

Figure 2. Scaling predictions at 90% recovery using AWC Proton software based on 0.75 ppm AWC A-119 (green: minimum 2 h to failure; yellow: minimum <2−1 h to failure; orange: <1 h to failure; red: instant failure).

to meet the minimum requirement of concentrate rate. Design calculations at steady-state have been reported previously,[34] which shows that the energy consumption of the three-stage system at 90% recovery is only a few percent higher than the one of the original two-stage system at 80%. As a result, the SEC of the new system is even smaller.

The main constituents and their average concentrations in mg/L of the feedwater to Chino I are as follows:[39] silica = 37, calcium = 174, magnesium = 40, barium = 0.2, strontium = 1.3, sulfate = 55, fluoride = 0.2, and nitrate = 170. The total dissolved solids (TDS) is 950 mg/L. Pretreatment before RO includes acid addition to lower the pH of the feed to 6.5 and dosing of scalant inhibitors.[12] At 90% recovery, the scale-forming compounds and their saturation indices (SI) predicted by the AWC's Proton Membrane Aqueous Chemistry Calculator[40] are shown in Figure 2. Dosing of 0.75 ppm AWC A-119 antiscalant can delay the scaling formation for at least 2 h.[41] Silica and the antiscalant itself are the most likely scaling components.

To further mitigate scaling at such a high recovery, membrane flushing features are added to process design and operation. Since FRRO and VCRO are essentially steady-state multistage RO most of the time, the focus of this work is to show the difference in process dynamics during the transition steps. The dimensionless spatiotemporal RO model used for the simulation is below[42]

$$
\begin{aligned}
0 &= \frac{\partial q^*}{\partial x^*} + \frac{\gamma_0}{1 + \frac{L_p \pi_0}{k_m} c^*}(\theta - c^*) \\
\frac{\partial c^*}{\partial t^*} &= -q^* \frac{\partial c^*}{\partial x^*} - c^* \frac{\partial q^*}{\partial x^*} + \frac{1}{Pe_D} \frac{\partial^2 c^*}{\partial x^{*2}} \\
0 &= \frac{\partial \theta}{\partial x^*} + \frac{a_2}{\pi_0} q^{*n_2}
\end{aligned} \tag{1}
$$

where q^* is the flow rate in the feed channel (Q) divided by the inlet flow rate at steady state (Q_0). c^* is the salt concentration (C) normalized by the inlet concentration at steady state (C_0). θ is the transmembrane pressure (ΔP) divided by the inlet osmotic pressure at steady state (π_0). t^* is the actual time t divided by the space time τ ($\tau = Q_0/V_c$, where V_c is the void volume in the RO feed channel. Based on an estimated void space of 0.012 m^3 in the feed channel of each RO element,[43] the space time is 0.41, 0.47, and 0.54 min for stages 1, 2, and 3 respectively). $x^* = x/L$ is the dimensionless length with 0 and 1 representing the entrance and outlet of the RO stage, respectively. L is the length of a pressure vessel, which is about 1 m for each RO element. γ_0 is a dimensionless parameter ($\gamma_0 = A_m L_p \pi_0 / Q_0$, where A_m is the membrane area per vessel and L_p is membrane hydraulic permeability). $k_m = a_1 q^{*n1}$ is the mass transfer coefficient, which varies as a function of the cross velocity. Pe_D is the dispersive Peclet number. a_1, n_1 and a_2, n_2 are parameters that characterize mass transfer and pressure drop.[37] The model is based on the following assumptions: (1) the salt rejection of the membrane is 100%, (2) the concentration polarization factor CPF = $\exp(J_w/k_m) \approx 1 + J_w/k_m$, and (3) the residence time distribution can be reasonably described by the dispersion model.[44] Details about the model development and numerical solution method can be found in a previous study.[42] The modeling parameters were validated for a wide range of recoveries (78−90%) in a series of plant experiments at Chino I each lasting about 15 min to minimize potential scaling damage to membranes.[4,36,37] A summary is provided in the Supporting Information. This spatiotemporal model has been recently applied to CCRO,[32] improved CCRO,[23] and a hybrid system consisting of the original CCRO and the improved CCRO.[43]

The boundary conditions for eq 1 depend on how the system is operated. Two simple cases are considered here. If the recovery (Y) in each stage is fixed during the transition steps, the boundary conditions are as follows

https://doi.org/10.1021/acs.iecr.3c04406
Ind. Eng. Chem. Res. 2024, 63, 5813−5822

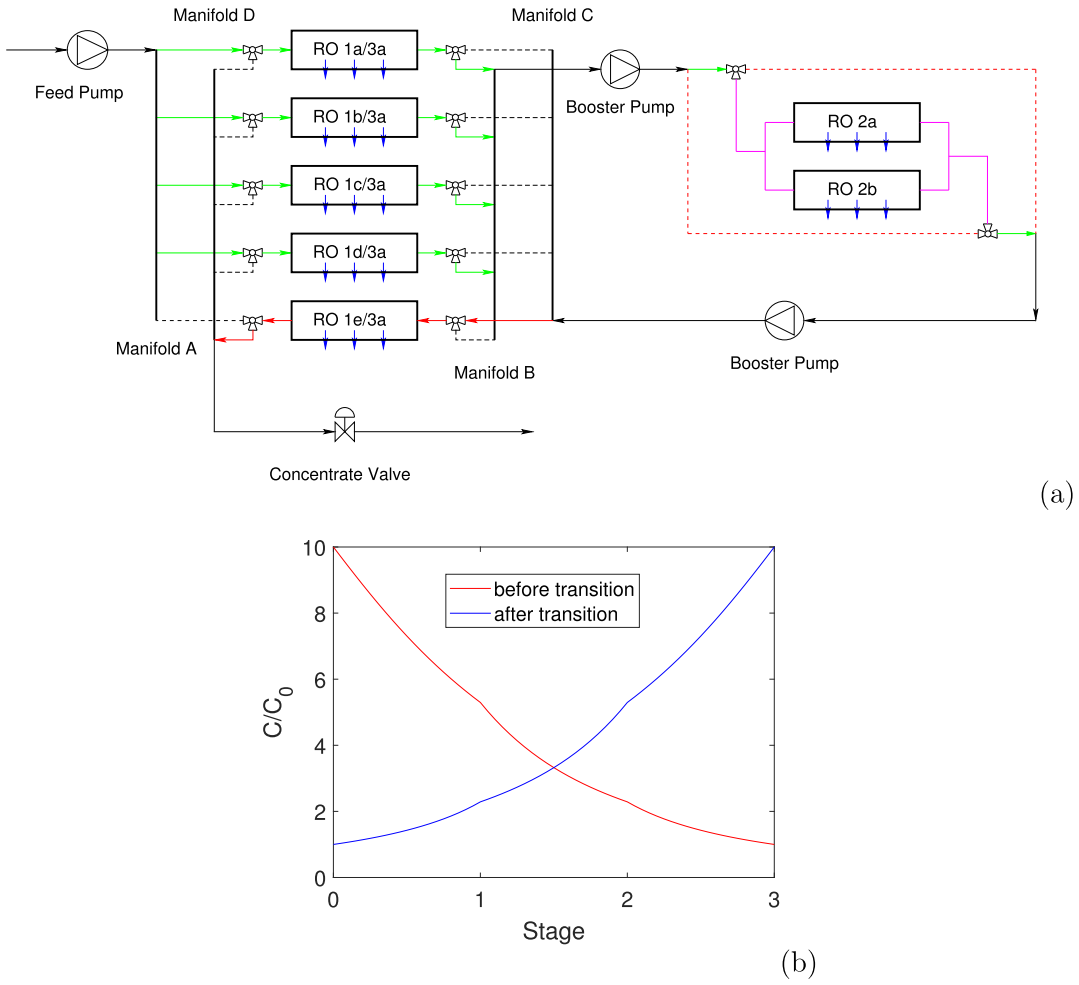

Figure 3. (a) Schematic of FRRO showing block rotation and flow reversal characteristics. (b) Spatial salt concentration profile before and after block rotation and flow reversal in FRRO.

$$
\begin{aligned}
q^*(x^*, t^*)|_{x^*=0} &= 1\\
q^*(x^*, t^*)|_{x^*=1} &= 1 - Y\\
\left(c^* - \frac{1}{Pe_D}\frac{\partial c^*}{\partial x^*}\right)\Big|_{x^*=0^+} &= c^*(x^*, t^*)|_{x^*=0^-}\\
\left.\frac{\partial c^*}{\partial x^*}\right|_{x^*=1} &= 0\\
\theta'(x^*, t^*)|_{x^*=0} &= -\frac{a_2}{\pi_0}\\
\theta'(x^*, t^*)|_{x^*=1} &= -\frac{a_2}{\pi_0}(1 - Y)^{n_2}
\end{aligned}
\tag{2}
$$

If the feed pressure in each stage is fixed during the transition, the boundary conditions are

$$
\begin{aligned}
q^*(x^*, t^*)|_{x^*=0} &= q^*(0, t^*)\\
(q^*)'(x^*, t^*)|_{x^*=0} &= -\frac{\gamma_0}{1 + \frac{L_p\pi_0}{k_m}c^*(0^+, t^*)}(\theta(0, t^*) - c^*(0^+, t^*))\\
\left(c^* - \frac{1}{Pe_D}\frac{\partial c^*}{\partial x^*}\right)\Big|_{x^*=0^+} &= c^*(x^*, t^*)|_{x^*=0^-}\\
\left.\frac{\partial c^*}{\partial x^*}\right|_{x^*=1} &= 0\\
\theta(x^*, t^*)|_{x^*=0} &= \theta(0, t^*)\\
\theta'(x^*, t^*)|_{x^*=0} &= -\frac{a_2}{\pi_0}
\end{aligned}
\tag{3}
$$

Figure 3a shows a schematic of FRRO with a 4:2:1 RO array following ROTEC's concept. At any moment, 4 out of 5 RO blocks (RO1a/3a, RO1b/3a, RO1c/3a, RO 1d/3a, and RO1e/3a) on the left of Figure 3a are stage 1 while the remaining one serves as stage 3. The 2 blocks (RO2a and RO2b) on the right of Figure 3a form stage 2. The flow direction to block(s) is forward

https://doi.org/10.1021/acs.iecr.3c04406
Ind. Eng. Chem. Res. 2024, 63, 5813−5822

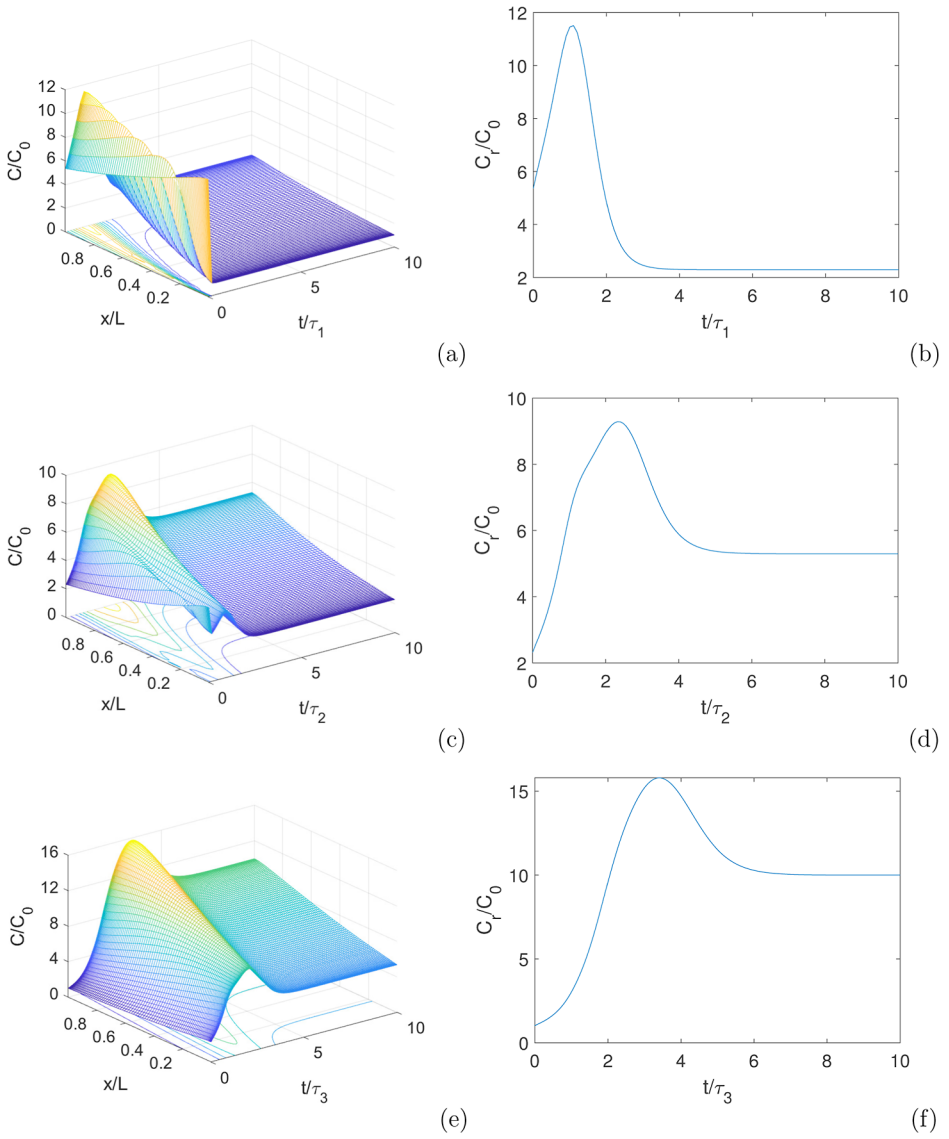

Figure 4. (a,c,e) Spatiotemporal salt concentration profile and (b,d,f) brine salt concentration in each stage during block rotation and flow reversal in FRRO. τ_1, τ_2, and τ_3 are space times for stage 1, 2, and 3, respectively. Recovery of each stage is fixed during the transition.

in stage 1 and reverse in stage 3. It can be either forward or reverse in stage 2. Periodically, block rotation and flow reversal occur in stages 1 and 3. At the same time, feed flow to the blocks in stage 2 changes in direction. During the transition period, the spatial concentration profile in the whole system (except for 3 blocks in stage 1 that remain in the same positions during block rotation) is completely flipped, as shown in Figure 3b. This leads to a propagating concentration wave traveling across the entire system, as shown in Figure 4.

When the block in stage 3 is repositioned in stage 1, the element associated with the highest concentration ($10C_0$) is facing the fresh feed while the rear element has the lowest concentration ($5.3C_0$). The initial salt load is much higher than its value after the transition is complete. The interplay among convection, backmixing (or axial dispersion), and filtration results in a concentration peak traveling downstream (Figure 4a). A concentration overshoot is expected at the end of this block (greater than $11C_0$ in this case) before the steady state is reached (Figure 4b). The magnitude of the concentration peak is lowered to approximately $4.5C_0$ at the end of stage 1 due to the blending of retentate streams from this block and three other blocks that remain in stage 1 during the transition.

The mixture of retentate streams from four blocks in stage 1 now enters stage 2, whose initial spatial profile of salt concentration is flipped, i.e., the highest at the entrance ($5.3C_0$) and the lowest at the outlet ($2.3C_0$). The magnitude of the concentration wave generated from stage 1 is in between these two levels. As a result, the salt concentration at the entrance of stage 2 reduces initially. It starts to increase as the peak of the concentration wave (Figure 4b) approaches the entrance. After the wave travels further downstream, the concentration at the inlet of stage 2 gradually decreases to its steady state value ($2.3C_0$). Because the feed concentration is higher than normal for a period of time, a concentration overshoot at the end of stage 2 is inevitable. However, it is less than $10C_0$.

Finally, the concentration wave from the end of stage 2 passes through stage 3, whose initial concentration is also spatially flipped but is at low levels, i.e., the highest ($2.3C_0$) at the entrance and the lowest (C_0) at the outlet. Because the inlet concentration is greater than $5.3C_0$ for a period of time, another

https://doi.org/10.1021/acs.iecr.3c04406
Ind. Eng. Chem. Res. 2024, 63, 5813−5822

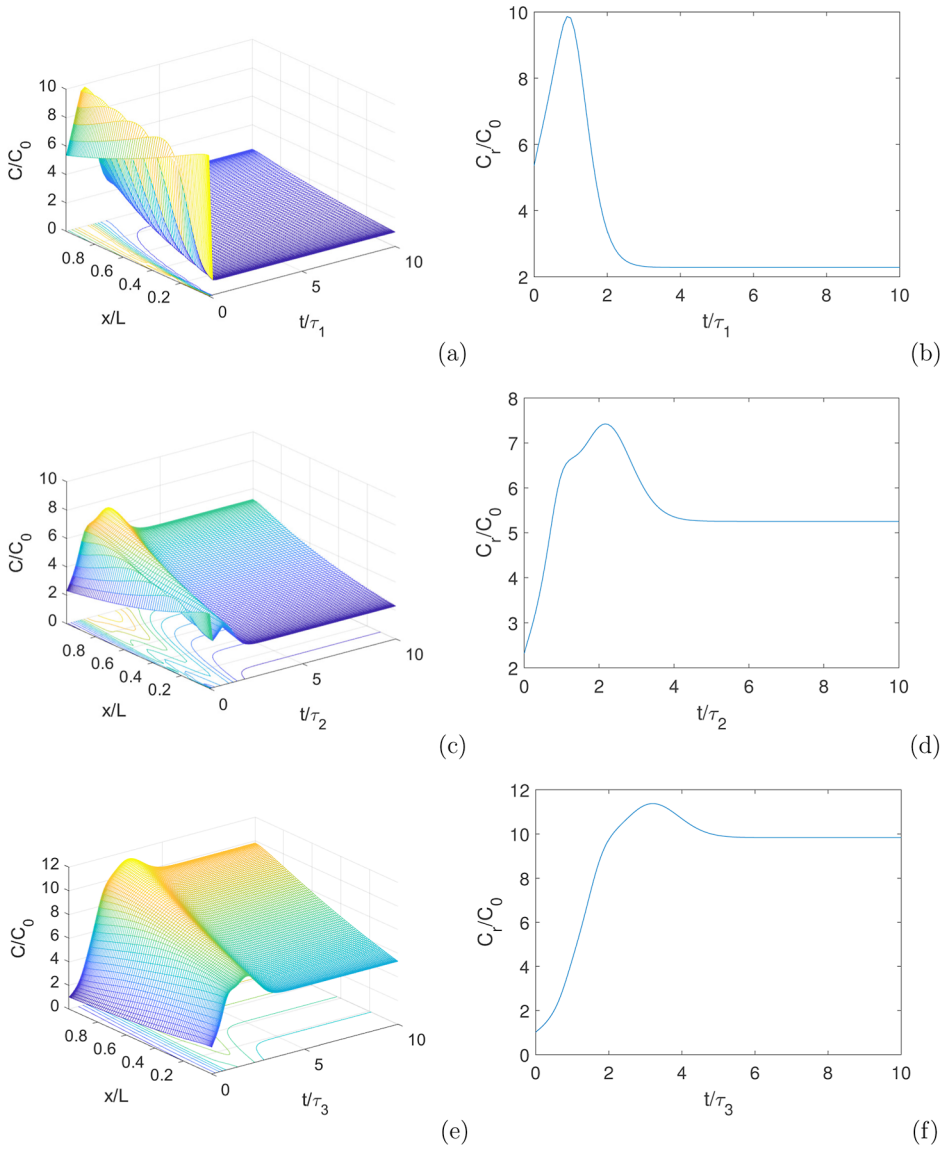

Figure 5. (a,c,e) Spatiotemporal salt concentration profile and (b,d,f) brine salt concentration in each stage during block rotation and flow reversal in FRRO. τ_1, τ_2, and τ_3 are space times for stage 1, 2, and 3, respectively. Pressure at each stage is fixed during the transition.

concentration overshoot (greater than $10C_0$) occurs at the outlet. In fact, it is found that the areas bounded by the curves below and above the line $C_r/C_0 = 10$ in Figure 4f are equal. In other words, the time average of the brine concentration is $10C_0$ to maintain a constant recovery of 90%.

Even though ROTEC's FRRO balances salt load among all blocks in stages 1 and 3, the simulation shows that there might be concentration hotspots during transition steps. In pilot tests of ROTEC's FRRO with a 3:2:1 array at the Arcadia plant, a significant concentration overshoot is observed every time that blocks rotation and flow reversal occur at the same time. Moreover, the specific flux (or membrane permeability) in stages 1 and 3 decays at a faster rate than that in stage 2.[31] One plausible reason is that stages 1 and 3 periodically treat the most aggressive water. In addition, it is postulated that these concentration hotspots may deteriorate the formation of scaling. One possible way to reduce them is to temporarily lower the recovery of each stage during the transition. Figure 5 shows the simulation results using eq 3 as boundary conditions. By applying the same applied pressures at the steady state during the transition steps, the driving force (or the difference between transmembrane hydraulic pressure and transmembrane osmotic pressure) is smaller initially and gradually increases as the concentration peak passes by. It is shown that the concentration hotspots are somewhat suppressed but are not eliminated. Clearly, a smart control system may be required for a smooth transition at the expense of production loss.

In VCRO, the FRRR unit is disconnected from the multistage subsystem, flushed using the fresh feed, and then reinstated for full production. If the feed direction is reversed during the flushing step, a similar concentration wave would propagate along the FRRR subsystem without negatively impacting the multistage RO subsystem. Two cases, corresponding to 0 and 50% recovery during the flushing step, are shown in Figures 6 and 7, respectively. When $Y = 0\%$, the concentration level during the transition is lower. Moreover, reverse flux may occur in some part of the membrane (Figure 8), which would loosen foulants/scalants from the membrane surface.[32] One obvious drawback is the production loss during this period. When $Y = 50\%$, the production loss is smaller; however, the concentration is higher

https://doi.org/10.1021/acs.iecr.3c04406
Ind. Eng. Chem. Res. 2024, 63, 5813−5822

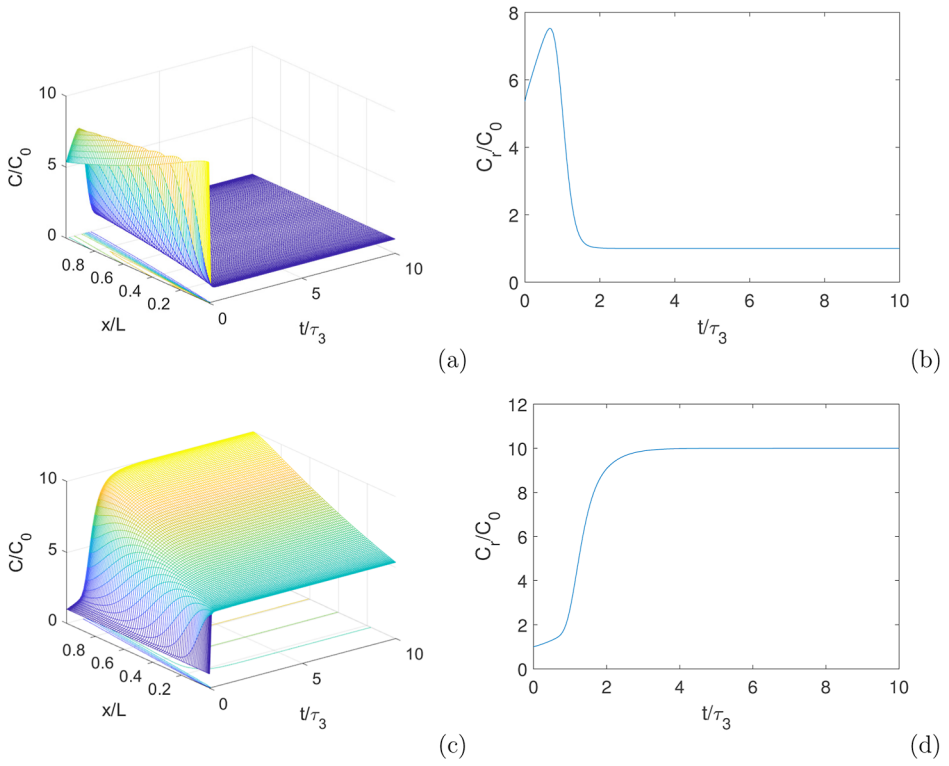

Figure 6. (a,c) Spatiotemporal salt concentration profile and (b,d) brine concentration in the last stage during flushing and full production in VCRO. Recovery rate is set to be 0% during the flushing step.

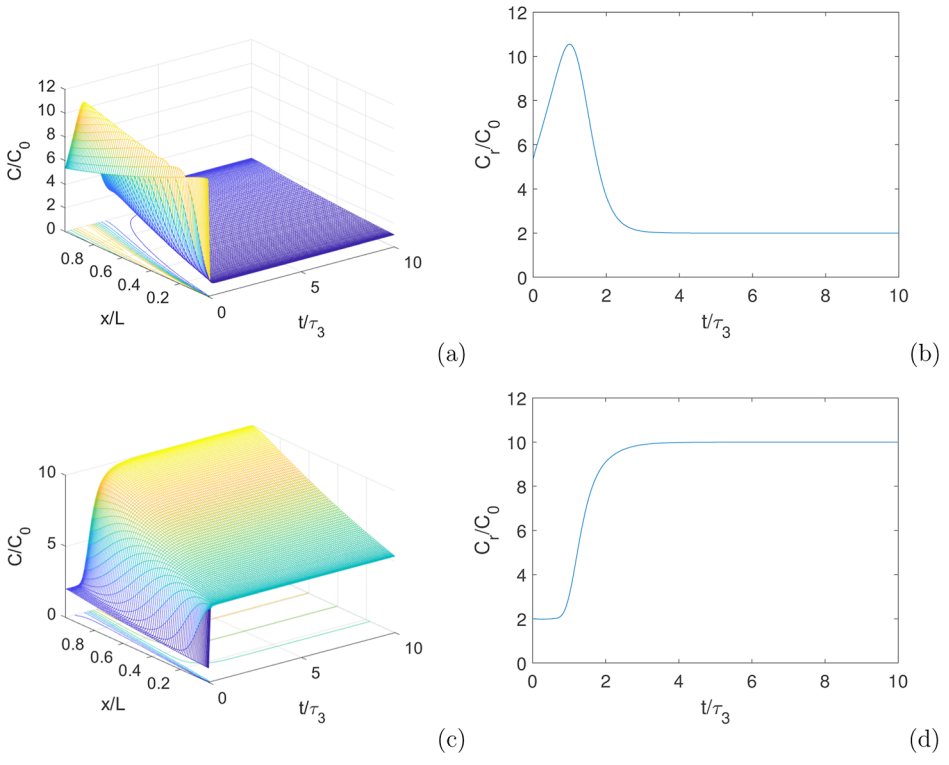

Figure 7. (a,c) Spatiotemporal salt concentration profile and (b,d) brine concentration in the last stage during flushing and full production in VCRO. Recovery rate is set to be 50% during the flushing step.

during the transition and may exceed $10C_0$ for a short period of time. An estimate of the overall recovery is shown in Table 3. On the basis of a 60 min full production step followed by a 4 min partial production and flushing step, the time-average recovery is 89.0% (Y = 50% in flushing of FRRR) or 88.4% (Y = 0% in flushing of FRRR). If the full production step can be extended to 120 min and the flushing step can be shortened to 2 min, then the average recovery is very close to 90% in both cases. The SEC

https://doi.org/10.1021/acs.iecr.3c04406
Ind. Eng. Chem. Res. 2024, 63, 5813−5822

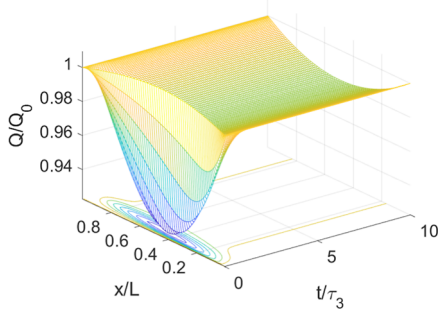

Figure 8. Spatiotemporal profile of flow in the FRRR subsystem during flushing without filtration flux.

Table 3. Overall Recovery Rate

	flow	recovery	duration (min)	
in series	Q_0	90%	60	120
in parallel	Q_0	81%	4	2
	$0.19Q_0$	50% (0%)	4	2
overall recovery			89.0% (88.4%)	89.7% (89.6%)

for all the cases listed in Table 3 is no more than 0.435 kW h/m^3 assuming a constant 80% pump efficiency. This is less than 1% different from the SEC in the conventional three-stage system at the same recovery (0.433 kW h/m^3).[34] The difference is minor mainly because the flushing step is short, and the flow rate of the flushing fluid is small. When the retentate cycle is turned on for the sake of boosting cross velocity, the energy consumption may increase by a few percent, depending on the recycle ratio.[34] The FRRO pilot study using Toray TML10D membranes at the Arcadia plant (feed TDS is approximately 1000 mg/L) had a SEC of 0.41−0.49 kW h/m^3 (assuming 80% pump efficiency) at 90% recovery.[31] The SEC levels in both cases appear to be similar.

One may conjecture that ROTEC's FRRO has a longer CIP interval relative to VCRO because 5 out of 7 pressure vessels (on the basis of a 4:2:1 array) equally share the contact time with the highest salt concentration. Whereas in VCRO, both ends of the same pressure vessel are each exposed to the highest salt concentration 50% of the time. However, it is clear from the simulations that the concentration hotspots can be effectively suppressed during the flushing step in VCRO. Moreover, the multistage subsystem may still operate at an 80% recovery if the FRRR subsystem must be turned offline for cleaning. Therefore, the downtime for the VCRO may be shorter. Additionally, VCRO is a much simpler design than ROTEC's FRRO, therefore, has less chance of equipment failure, and requires a smaller capital investment for plant retrofit. A comprehensive experimental study is recommended for a detailed comparison of both techniques.

CONCLUSIONS

A variable configuration RO is proposed for ultrahigh recovery applications. The two subsystems periodically switch between in-series configuration for high recovery operation and in-parallel configuration for reduced recovery and flushing of the most concentrated membranes using the under-saturated feed. This circumvents a high concentration wave prorogating across all RO stages in ROTEC's FRRO. The open-circuit design also avoids salt retention seen in CCRO/BRO. The SEC is estimated to be 0.45 kW h/m^3 at 90% recovery based on design conditions used in this work. A comprehensive experimental investigation is recommended to establish the scaling propensity and CIP frequency in VCRO relative to ROTEC's FRRO.

ASSOCIATED CONTENT

Supporting Information

The Supporting Information is available free of charge at https://pubs.acs.org/doi/10.1021/acs.iecr.3c04406.

(PDF)

AUTHOR INFORMATION

Corresponding Authors

Mingheng Li − *Department of Chemical and Materials Engineering, California State Polytechnic University, Pomona, California 91768, United States;* orcid.org/0000-0002-6611-425X; Phone: +1-909-869-3668; Email: minghengli@cpp.edu; Fax: +1-909-869-6920

Joseph Li − *Department of Chemical and Biomolecular Engineering, University of California, Berkeley, California 94720, United States*; Email: lijoseph@berkeley.edu

Complete contact information is available at: https://pubs.acs.org/10.1021/acs.iecr.3c04406

Notes

The authors declare no competing financial interest.

ACKNOWLEDGMENTS

The corresponding author would like to acknowledge financial support from the National Science Foundation (CBET-2140946) and the National Alliance for Water Innovation, Department of Energy (7722635). Any opinions, findings, conclusions, or recommendations expressed in this material are those of the authors and do not necessarily reflect the views of the funders.

REFERENCES

(1) Elimelech, M.; Phillip, W. A. The future of seawater desalination: Energy, technology, and the environment. *Science* **2011**, *333*, 712−717.

(2) Burn, S.; Gray, S. *Efficient Desalination by Reverse Osmosis: A Guide to RO Practice*; IWA Publishing: London, UK, 2016.

(3) Qasim, M.; Badrelzaman, M.; Darwish, N. N.; Darwish, N. A.; Hilal, N. Reverse osmosis desalination: A state-of-the-art review. *Desalination* **2019**, *459*, 59−104.

(4) Li, M.; Noh, B. Validation of model-based optimization of brackish water reverse osmosis (BWRO) plant operation. *Desalination* **2012**, *304*, 20−24.

(5) Gu, H.; Plumlee, M. H.; Boyd, M.; Hwang, M.; Lozier, J. C. Operational optimization of closed-circuit reverse osmosis (CCRO) pilot to recover concentrate at an advanced water purification facility for potable reuse. *Desalination* **2021**, *518*, 115300.

(6) Panagopoulos, A.; Haralambous, K.; Loizidou, M. Desalination brine disposal methods and treatment technologies - A review. *Sci. Total Environ.* **2019**, *693*, 133545.

(7) Sanciolo, P.; Milne, N.; Taylor, K.; Mullet, M.; Gray, S. Silica scale mitigation for high recovery reverse osmosis of groundwater for a mining process. *Desalination* **2014**, *340*, 49−58.

(8) Antony, A.; Low, J. H.; Gray, S.; Childress, A. E.; Le-Clech, P.; Leslie, G. Scale formation and control in high pressure membrane water treatment systems: A review. *J. Membr. Sci.* **2011**, *383*, 1−16.

(9) Amjad, Z. Scale inhibition in desalination applications: an overview. *The NACE International Annual Conference and Exposition*; Corrosion, 1996, p NACE-96-230.

(10) Matin, A.; Rahman, F.; Shafi, H. Z.; Zubair, S. M. Scaling of reverse osmosis membranes used in water desalination: Phenomena,

impact, and control; future directions. *Desalination* **2019**, *455*, 135−157.
(11) Rolf, J.; Cao, T.; Huang, X.; Boo, C.; Li, Q.; Elimelech, M. Inorganic scaling in membrane desalination: models, mechanisms, and characterization methods. *Environ. Sci. Technol.* **2022**, *56*, 7484−7511.
(12) Li, M. *Analysis and Design of Membrane Processes: A Systems Approach*; AIP Publishing: Melville, NY, 2020.
(13) Efraty, A.; Septon, J. Closed circuit desalination series no-5: high recovery, reduced fouling and low energy nitrate decontamination by a cost-effective BWRO-CCD method. *Desalin. Water Treat.* **2012**, *49*, 384−389.
(14) Sonera, V.; Septon, J.; Efraty, A. CCD series no-21: illustration of high recovery (93.8%) of a silica containing (57 ppm) source by a powerful technology of volume reduction prospects. *Desalin. Water Treat.* **2016**, *57*, 20228−20236.
(15) Werber, J. R.; Deshmukh, A.; Elimelech, M. Can batch or semi-batch processes save energy in reverse-osmosis desalination? *Desalination* **2017**, *402*, 109−122.
(16) Boyd, M. Closed circuit reverse osmosis, the new standard for industrial desalination. 2019, https://www.kansaswatertech.com/includes/newsletters/2019/05/CCRO_TheNewStandard.pdf (accessed Mar 23, 2023).
(17) Lee, T.; Rahardianto, A.; Cohen, Y. Multi-cycle operation of semi-batch reverse osmosis (SBRO) desalination. *J. Membr. Sci.* **2019**, *588*, 117090.
(18) Nayar, K. G.; Lienhard V, J. H. Brackish water desalination for greenhouse agriculture: Comparing the costs of RO, CCRO, EDR, and monovalent-selective EDR. *Desalination* **2020**, *475*, 114188.
(19) Davies, P. A.; Wayman, J.; Alatta, C.; Nguyen, K.; Orfi, J. A desalination system with efficiency approaching the theoretical limits. *Desalin. Water Treat.* **2016**, *57*, 23206−23216.
(20) Warsinger, D. M.; Tow, E. W.; Nayar, K. G.; Maswadeh, L. A.; Lienhard V, J. H. Energy efficiency of batch and semi-batch (CCRO) reverse osmosis desalination. *Water Res.* **2016**, *106*, 272−282.
(21) Warsinger, D. M.; Tow, E. W.; Maswadeh, L. A.; Connors, G. B.; Swaminathan, J.; Lienhard V, J. H. Inorganic fouling mitigation by salinity cycling in batch reverse osmosis. *Water Res.* **2018**, *137*, 384−394.
(22) Li, M. Dynamic Operation of Batch Reverse Osmosis and Batch Pressure Retarded Osmosis. *Ind. Eng. Chem. Res.* **2020**, *59*, 3097−3108.
(23) Li, M. An improved Closed-Circuit RO (CCRO) system: Design and cyclic simulation. *Desalination* **2023**, *554*, 116519.
(24) Hosseinipour, E.; Karimi, S.; Barbe, S.; Park, K.; Davies, P. A. Hybrid semi-batch/batch reverse osmosis (HSBRO) for use in zero liquid discharge (ZLD) applications. *Desalination* **2022**, *544*, 116126.
(25) Lauer, G. Conditioning process and device for producing pure water. U.S. Patent 5,690,829 A, 1997.
(26) Pomerantz, N.; Ladizhansky, Y.; Korin, E.; Waisman, M.; Daltrophe, N.; Gilron, J. Prevention of scaling of reverse osmosis membranes by "zeroing" the elapsed nucleation time. Part I. Calcium sulfate. *Ind. Eng. Chem. Res.* **2006**, *45*, 2008−2016.
(27) Uchymiak, M.; Bartman, A. R.; Daltrophe, N.; Weissman, M.; Gilron, J.; Christofides, P. D.; Kaiser, W. J.; Cohen, Y. Brackish water reverse osmosis (BWRO) operation in feed flow reversal mode using an ex situ scale observation detector (EXSOD). *J. Membr. Sci.* **2009**, *341*, 60−66.
(28) Bartman, A. R.; McFall, C. W.; Christofides, P. D.; Cohen, Y. Model-predictive control of feed flow reversal in a reverse osmosis desalination process. *J. Process Control* **2009**, *19*, 433−442.
(29) Gu, H.; Bartman, A. R.; Uchymiak, M.; Christofides, P. D.; Cohen, Y. Self-adaptive feed flow reversal operation of reverse osmosis desalination. *Desalination* **2013**, *308*, 63−72.
(30) Erlitzki, R. High Recovery Flow Reversal Technology. 2019, https://www.usbr.gov/research/bgndrf/win2019/Erlitzki-WIN-2019.pdf (accessed Sep 1, 2021).
(31) Li, M.; Waite, A.; Wang, S. Piloting Experience of ROTEC's Flow Reversal RO (FRRO) for 90% Recovery in Brackish Water Desalination. *Desalination* **2024**, *576*, 117348.
(32) Li, M. Cyclic simulation and energy assessment of closed-circuit RO (CCRO) of brackish water. *Desalination* **2023**, *545*, 116149.
(33) Wang, S.; Waite, A. Personal communication, 2022.
(34) Li, M.; Chan, N.; Li, J. Novel Dynamic and Cyclic Designs for Ultra-High Recovery Waste and Brackish Water RO Desalination. *Chem. Eng. Res. Des.* **2022**, *179*, 473−483.
(35) Waite, A.; Broley, W.; Ingalsbe, M.; Wang, S.; Trussell, B. Can Closed Circuit Desalination Boost Brackish Groundwater and Recycled Water Recovery by Squeezing Concentrate?. *AWWA California-Nevada Section Annual Fall Conference*; AWWA: Rancho Mirage, CA, 2018.
(36) Li, M. Optimal plant operation of brackish water reverse osmosis (BWRO) desalination. *Desalination* **2012**, *293*, 61−68.
(37) Li, M.; Bui, T.; Chao, S. Three-dimensional CFD analysis of hydrodynamics and concentration polarization in an industrial RO feed channel. *Desalination* **2016**, *397*, 194−204.
(38) Dupont. FilmTec Reverse Osmosis Membranes Technical Manual. 2020, https://www.dupont.com/content/dam/dupont/amer/us/en/water-solutions/public/documents/en/45-D01504-en.pdf (accessed Apr 25, 2020).
(39) Inland Empire Utilities Agency. *Chino I Desalter Operation and Maintenance Manual*; Inland Empire Utilities Agency, 2005.
(40) https://www.awcproton.com (accessed Sep 12, 2023).
(41) Utter, J.; Lovell, N. Personal communication, 2023.
(42) Li, M. A. A spatiotemporal model for dynamic RO simulations. *Desalination* **2021**, *516*, 115229.
(43) Li, M. Effect of Cylinder Sizing on Performance of Improved Closed-Circuit RO (CCRO). *Desalination* **2023**, *561*, 116688.
(44) Li, M. Residence Time Distribution in RO Channel. *Desalination* **2021**, *506*, 115000.

https://doi.org/10.1021/acs.iecr.3c04406
Ind. Eng. Chem. Res. 2024, 63, 5813−5822